AN ANALYTICAL STUDY ON PIEZOELECTRIC-BISTABLE LAMINATES WITH ARBITRARY SHAPES FOR ENERGY HARVESTING

S. Mehdi Tavakkoli[*], Paul M. Weaver[†], Christopher R. Bowen[*], Daniel J. Inman[††], H. Alicia Kim[*]

[*]Department of Mechanical Engineering, University of Bath
Bath, BA2 7AY, UK
s.m.tavakkoli@bath.ac.uk
c.r.bowen@bath.ac.uk
h.a.kim@bath.ac.uk

[†]National Physical Laboratory,
Teddington, TW11 0LW, UK
paul.weaver@npl.co.uk

[††]Department of Aerospace Engineering, University of Michigan,
Ann Arbor, MI, 48109, USA
daninman@umich.edu

Key words: Bistable laminates, Piezoelectric, Energy harvesting.

Summary: *Due to large deformations of bi-stable laminates arising from asymmetric lay-ups, they have been identified as good candidates to combine with piezoelectrics for broadband energy harvesting. Fast transitions from one stable state to another, or 'snap-through', is used to repeatedly deform the surface-bonded piezoelectric and generate large strains hence electrical energy. Existing studies, both experimental and numerical, have been limited to laminates of rectangular shapes. This paper investigates the mechanical behavior and energy harvesting potential of a nonrectangular shape composite by developing an analytical model for piezoelectric-bistable laminates with arbitrary shapes. The electromechanical governing equations of the system are derived based on Hamilton's principle and solved using the Runge-Kutta method. In order to model arbitrary shapes, the domain of interest is discretized into small elements and the density of each element is considered to be one for solid areas and zero for voids; the stiffness of the void elements are assumed to be zero. In order to verify the model, the obtained results are compared with experimental measurements. The effects of using different laminate geometries on harvested power are discussed by considering square and cruciform cross-shaped examples.*

1 INTRODUCTION

Vibration-based energy harvesting for low-powered electronics has received significant interests in recent years as solutions are sought to provide remote sources of power for applications such as wireless sensor networks or safety monitoring devices. While energy

S. Mehdi Tavakkoli, Paul M. Weaver, Christopher R. Bowen, Daniel J. Inman, H. Alicia Kim

harvesters are often tuned to operate near resonance, many typical vibration patterns are composed of multiple frequencies across a wide band [1-3]. For efficient energy harvesting it is necessary to tune the operating frequencies, typically achieved through geometry and mass variation, and to broaden the frequency bandwidth by introducing stiffness nonlinearities, typically achieved through the use of external magnets [4]. A solution which allows design for both mass distribution and specific nonlinear stiffness characteristics through variation in geometric variables is desirable. One approach is to exploit bistability in composite laminates with an asymmetric stacking sequence. The advantage of this approach is that it removes the need for external components. It is well known that composite laminates with asymmetric stacking sequences can exhibit two curved stable shapes due to the mismatch in thermal properties between plies and the temperature change experienced during manufacture [5]. This property makes them suitable for piezoelectric energy harvesting by utilizing a snap-through mechanism between the two stable states to repeatedly strain a surface-bonded piezoelectric, such as a Macro Fibre Composite (MFC).

Significant power outputs over a wide bandwidth have been reported using square bistable laminates [6]. The full potential for improving the power generation of bistable laminate energy harvesters and to reduce the mechanical energy input required to induce snap-through has yet to be exploited since existing designs have been limited to square and rectangular laminate shapes [6-8].

Static modelling of the stable shapes of square bistable laminates is well established [5,9], in which the curved shapes of asymmetric laminates due to the high temperatures experienced during manufacturing (curing process) are modelled based on a nonlinear extension to classical laminated plate theory. The midplane strains and out-of-plane displacement profile are assumed to conform to second order polynomials. The process of identifying the static stable shapes is performed by identifying the values of the coefficients of these assumed polynomials through minimization of the total strain energy. This modelling approach has been validated experimentally and using finite element analysis for square and rectangular laminates [9-11]. We have previously mapped this static modelling to a dynamics model including piezoelectric elements for energy harvesting by characterizing the double-well potential energy of the system [12]. This model provides a prediction of power outputs for any given vibration pattern, captures the full range of dynamic modes seen experimentally, and the boundaries between these modes, limited to square laminates. The cured shapes of bistable laminates of trapezoidal and triangular planform have been considered experimentally and modelled using finite element analysis [13] for morphing applications, and have been modelled analytically in tapered cantilever configurations [14]. However, to date, no analytical model of the stable shapes of any profile, referred to in this work as 'arbitrary geometry' laminates, has been presented.

In this paper, an analytical model for arbitrary shape piezoelectric-bistable laminates is developed. The electromechanical nonlinear governing equations of the system are derived through the sections 2, 3 and 4. Section 5 is devoted to introduce a simple technique to model arbitrary shapes. To achieve this, the domain of interest is discretized into small elements and the density of each element is considered to be one for solid areas and zero for voids; the stiffness of the void elements are assumed to be zero. Figure 1 shows an example arbitrary geometry laminate centrally mounted on an electrodynamic shaker. Attached to the surface of the laminate is a small rectangular piezoelectric MFC. The results of the model are demonstrated in section 6 and compared with experimental tests in section 7.

Figure 1. A cruciform (+ shape) arbitrary shaped $[0/90]_T$ laminate. Overall laminate dimension is 150×150mm. A piezoelectric element is attached to the surface of the laminate.

2 CONSTITUTIVE EQUATIONS FOR PIEZOELECTRIC LAYER

In general, constitutive equations for piezoelectric materials are divided into direct and converse effects and may be expressed as,

$$\begin{cases} \boldsymbol{\sigma} = \mathbf{C}\boldsymbol{\varepsilon} - \mathbf{e}\,\mathbf{E} \\ \mathbf{D} = \mathbf{e}\boldsymbol{\varepsilon} + \boldsymbol{\eta}\mathbf{E} \end{cases} \tag{1}$$

respectively, where $\boldsymbol{\sigma}$ and $\boldsymbol{\varepsilon}$ are stress and strain fields, respectively, $\mathbf{C}$ is the elasticity matrix, $\mathbf{e}$ is the electromechanical coupling coefficients matrix, $\mathbf{E}$ is the electrical field vector, $\mathbf{D}$ is the electrical displacement vector and $\boldsymbol{\eta}$ is the permittivity matrix.

In this work, the piezoelectric plate is assumed to be polarized in the thickness direction $e_{36}=0$ and the electrical and displacement fields are uniform across the thickness and aligned in the direction normal to the mid-plane $D_1=D_2=0$. In addition, by assuming $\sigma_{33}=0$ for plate structures and using the Kirchhoff plate theory, the constitutive relation can be summarized and expanded as follows,

$$\begin{bmatrix} \sigma_{11} \\ \sigma_{22} \\ \sigma_{12} \\ D_3 \end{bmatrix} = \begin{bmatrix} C_{11} & C_{12} & C_{16} & e_{31} \\ C_{21} & C_{22} & C_{26} & e_{32} \\ C_{61} & C_{62} & C_{66} & 0 \\ e_{31} & e_{32} & 0 & -\eta_{33} \end{bmatrix} \begin{bmatrix} \varepsilon_{11} \\ \varepsilon_{22} \\ \varepsilon_{12} \\ -E_3 \end{bmatrix} \tag{2}$$

Since the Kirchhoff theory is used, shear forces perpendicular to the mid plane are assumed to be negligible. Axial forces $\mathbf{N}$ and bending moments $\mathbf{M}$ are defined by the expressions,

$$\mathbf{N} = \langle N_{11} \quad N_{22} \quad N_{12} \rangle^T = \int_{t_1^p}^{t_2^p} \boldsymbol{\sigma}^0 \, dz$$

$$\mathbf{M} = \langle M_{11} \quad M_{22} \quad M_{12} \rangle^T = \int_{t_1^p}^{t_2^p} z \, \boldsymbol{\sigma} \, dz \tag{3}$$

where $t_2^p - t_1^p$ is the thickness of the piezoelectric layer, z is the axis along the thickness and $\boldsymbol{\sigma}^0$ and $\boldsymbol{\sigma}$ are the membrane and bending parts of section stress defined as,

$$\boldsymbol{\sigma}^0 = \mathbf{C}\boldsymbol{\varepsilon}^0 \; ; \; \boldsymbol{\sigma} = z\mathbf{C}\boldsymbol{\kappa} \tag{4}$$

where $\boldsymbol{\varepsilon}^0$ and $\boldsymbol{\kappa}$ are the in-plane strains and curvatures, respectively.

By substituting (2) into (3), the actuating equation for a cross-ply laminate in a general and compact form may be expressed as,

$$\begin{bmatrix} \mathbf{N} \\ \mathbf{M} \end{bmatrix} = \begin{bmatrix} \mathbf{A} & \mathbf{B} \\ \mathbf{B} & \mathbf{D} \end{bmatrix} \begin{bmatrix} \boldsymbol{\varepsilon}^0 \\ \boldsymbol{\kappa} \end{bmatrix} - (t_2^p - t_1^p) \begin{bmatrix} \mathbf{I}_3 \\ \dfrac{(t_2^p + t_1^p)}{2}\mathbf{I}_3 \end{bmatrix} \begin{bmatrix} e_{31} \\ e_{32} \\ 0 \end{bmatrix} E_3 \tag{5}$$

where $\mathbf{A}$, $\mathbf{D}$ and $\mathbf{B}$ are the membrane (extensional), bending and coupling stiffness matrices, respectively, and $\mathbf{I}_3$ is the identity matrix.

By integrating from both sides of the sensing equation over the thickness we obtain,

$$(t_2^p - t_1^p)D_3 = \begin{bmatrix} e_{31} & e_{32} & 0 \end{bmatrix} (t_2^p - t_1^p) \begin{bmatrix} \mathbf{I}_3 & \dfrac{(t_2^p + t_1^p)}{2}\mathbf{I}_3 \end{bmatrix} \begin{bmatrix} \boldsymbol{\varepsilon}^0 \\ \boldsymbol{\kappa} \end{bmatrix} + \eta_{33}E_3(t_2^p - t_1^p) \tag{6}$$

where the thickness can be cancelled from both sides and finally, the constitutive equations (1) are rewritten in a compact form for piezoelectric plate structures as follows,

$$\begin{cases} \overline{\mathbf{N}}^p = \mathbf{Q}^p\overline{\boldsymbol{\varepsilon}} - t^p\mathbf{e}'E_3 \\ D_3 = \mathbf{e}'^T\overline{\boldsymbol{\varepsilon}} + \eta_{33}E_3 \end{cases} \tag{7}$$

where,

$$\overline{\mathbf{N}}^p = \begin{bmatrix} \mathbf{N}^p \\ \mathbf{M}^p \end{bmatrix}, \quad \overline{\boldsymbol{\varepsilon}} = \begin{bmatrix} \boldsymbol{\varepsilon}^0 \\ \boldsymbol{\kappa} \end{bmatrix}, \quad \mathbf{Q}^p = \begin{bmatrix} \mathbf{A}^p & \mathbf{B}^p \\ \mathbf{B}^p & \mathbf{D}^p \end{bmatrix}, \quad \mathbf{e}' = \begin{bmatrix} \mathbf{I}_3 \\ \dfrac{\bar{t}}{2}\mathbf{I}_3 \end{bmatrix}\begin{bmatrix} e_{31} \\ e_{32} \\ 0 \end{bmatrix}, \quad \bar{t} = t_2^p + t_1^p, \quad t^p = t_2^p - t_1^p.$$

In geometrically nonlinear problems, it is convenient to separate the linear and nonlinear parts of strain field,

$$\overline{\boldsymbol{\varepsilon}} = \overline{\boldsymbol{\varepsilon}}^L + \overline{\boldsymbol{\varepsilon}}^{NL} \tag{8}$$

Therefore, the constitutive equations for geometrically nonlinear piezoelectric plates (7) can be expressed in terms of linear and nonlinear strains as follows,

$$\begin{cases} \overline{\mathbf{N}}^p = \mathbf{Q}^p\overline{\boldsymbol{\varepsilon}}^L + \mathbf{Q}^p\overline{\boldsymbol{\varepsilon}}^{NL} - t^p\mathbf{e}'E_3 \\ D_3 = \mathbf{e}'^T\overline{\boldsymbol{\varepsilon}}^L + \mathbf{e}'^T\overline{\boldsymbol{\varepsilon}}^{NL} + \eta_{33}E_3 \end{cases} \tag{9}$$

Similarly the constitutive equation for bistable laminates may be expressed as follows,

$$\overline{\mathbf{N}}^s = \mathbf{Q}^s\overline{\boldsymbol{\varepsilon}} \tag{10}$$

where superscript s stands for substructure. In addition, in order to examine the linear and nonlinear parts of the relation separately, using (8) we can write,

$$\overline{\mathbf{N}}^s = \mathbf{Q}^s\overline{\boldsymbol{\varepsilon}}^L + \mathbf{Q}^s\overline{\boldsymbol{\varepsilon}}^{NL} \tag{11}$$

3   APPROXIMATING FUNCTIONS

The in-plane strain field and out-of-plane displacement component (deflection) are approximated based on Hyer's model [9] which can be written in matrix form as,

$$\begin{bmatrix} \varepsilon_x^0 \\ \varepsilon_y^0 \\ \gamma_{xy}^0 \end{bmatrix} \approx \begin{bmatrix} 1 & x^2 & xy & y^2 & 0 & 0 & 0 & 0 & 0 & 0 \\ 0 & 0 & 0 & 0 & 1 & x^2 & xy & y^2 & 0 & 0 & 0 \\ 0 & 0 & \dfrac{x^2}{2} & 2xy & 0 & 2xy & \dfrac{y^2}{2} & 0 & 2 & x^2 & y^2 \end{bmatrix} \begin{bmatrix} d_1 \\ d_2 \\ \cdots \\ d_{11} \end{bmatrix} + \begin{bmatrix} 0 \\ 0 \\ f \end{bmatrix} = \overline{\varphi}\mathbf{d} + \mathbf{f} \approx \varepsilon^{0L} + \varepsilon^{0NL} \tag{12}$$

$$f(x,y,a,b,c) = (ab - \tfrac{1}{2}c^2)xy + \tfrac{1}{4}acx^2 + \tfrac{1}{4}bcy^2$$

$$w \approx \tfrac{1}{2}(ax^2 + by^2 + cxy) \tag{13}$$

where $d_1, \ldots, d_{11}$ are in-plane strain coefficients of the plate and a, b and c are curvature coefficients. Also, $\overline{\varphi}$ and $\mathbf{f}$ are the linear and nonlinear parts of the approximation functions in Hyer's model, respectively.

Using the in-plane strain field approximation in (12), $\overline{\varepsilon}^L$ and $\overline{\varepsilon}^{NL}$ from (8) may be expressed in terms of elongation coefficients $\mathbf{d}$ and curvature coefficients $\mathbf{a}$ in a matrix form as follows,

$$\overline{\varepsilon}^L = \begin{bmatrix} \varepsilon^{0L} \\ \kappa \end{bmatrix} \approx \begin{bmatrix} \overline{\varphi} & 0 \\ 0 & -\mathbf{I}_3 \end{bmatrix} \begin{bmatrix} \mathbf{d} \\ \mathbf{a} \end{bmatrix} = \mathbf{\Phi}\mathbf{X} \tag{14}$$

$$\overline{\varepsilon}^{NL} = \begin{bmatrix} \varepsilon^{0NL} \\ \mathbf{0} \end{bmatrix} \approx \begin{bmatrix} 0 & 0 & f & 0 & 0 & 0 \end{bmatrix}^T = \begin{bmatrix} \mathbf{f} \\ \mathbf{0} \end{bmatrix} \tag{15}$$

where $\mathbf{X}$ is the in-plane deformations and curvatures vector. The linear and nonlinear strains can be used for approximating internal forces in both the piezoelectric layer and bistable structure.

4 DYNAMIC GOVERNING EQUATIONS

To satisfy a dynamic equilibrium of the system based on a bistable laminate with bonded piezoelectric elements, the potential energy of the structure under dynamic conditions is minimized according to Hamilton's principle as follows,

$$\delta \int_{t_1}^{t_2} (T - U + W_{ie} + W_{nc})dt = 0 \tag{16}$$

where T is the kinetic energy, U is the strain energy, W_{ie} is the piezoelectric internal electrical energy and W_{nc} is the non-conservative works of the system. Each energy term in (16) is derived for a nonlinear piezoelectric composite plate in the following sections.

4.1 Strain Energy of the System, U

The strain energy of the system is calculated by adding the strain energies of the substructure and the piezoelectric layer. The substructure strain energy can be divided into mechanical and thermal strain energies. In the piezoelectric layer the converse piezoelectric component of the constitutive equation comprises two mechanical and electrical parts, therefore the piezoelectric strain energy may be separated into mechanical and electrical strain energies. Therefore, the total strain energy of the system may be written as follows,

$$U = U^s + U^p = U^{m,s} + U^{th,s} + U^{m,p} + U^{e,p} \tag{17}$$

where superscripts s, p, m, th, and e stand for substructure, piezoelectric, mechanical, thermal

and electrical strain energies, respectively. The substructure and piezoelectric strain energies may be expressed as,

$$U^s = U^{m,s} + U^{th,s} = \frac{1}{2}\int_{A^s} \overline{\mathbf{N}}^{s\,T}\overline{\boldsymbol{\varepsilon}}\,dA^s - \int_{A^s} \overline{\mathbf{N}}^{th\,T}\overline{\boldsymbol{\varepsilon}}\,dA^s \tag{18}$$

$$U^P = U^{m,p} + U^{e,p} = \frac{1}{2}\int_{A^p} \overline{\mathbf{N}}^{p\,T}\overline{\boldsymbol{\varepsilon}}\,dA^p \tag{19}$$

Substituting $\overline{\mathbf{N}}$ from constitutive equation (9) obtains,

$$U^s = U^{m,s} + U^{th,s} = \frac{1}{2}\int_{A^s} (\mathbf{Q}^s\overline{\boldsymbol{\varepsilon}}^L + \mathbf{Q}^s\overline{\boldsymbol{\varepsilon}}^{NL} - 2\mathbf{Q}^s\boldsymbol{\alpha}\,\Delta T)^T(\overline{\boldsymbol{\varepsilon}}^L + \overline{\boldsymbol{\varepsilon}}^{NL})\,dA^s \tag{20}$$

$$U^P = U^{m,p} + U^{e,p} = \frac{1}{2}\int_{A^p} (\mathbf{Q}^p\overline{\boldsymbol{\varepsilon}}^L + \mathbf{Q}^p\overline{\boldsymbol{\varepsilon}}^{NL} - t^p\mathbf{e}'E_3)^T(\overline{\boldsymbol{\varepsilon}}^L + \overline{\boldsymbol{\varepsilon}}^{NL})\,dA^p \tag{21}$$

where ΔT is the temperature change and $\boldsymbol{\alpha}$ is the thermal expansion coefficients vector.

Since the deformations and voltage are the unknowns in the above strain energy terms, the variation of the strain energy of the system in Hamilton's principle is calculated based on,

$$\delta U = \frac{\partial U}{\partial \mathbf{X}}\delta\mathbf{X} + \frac{\partial U}{\partial v}\delta v \tag{22}$$

where $\mathbf{X}$ is the in-plane deformations and curvature coefficients vector and v is the voltage.

4.2 Piezoelectric internal electrical energy, W_{ie}

The internal electrical energy W_{ie} in piezoelectric layer may be expressed as

$$W_{ie} = \frac{1}{2}\int_{A^p} \mathbf{E}^T\mathbf{D}\,dA^p \tag{23}$$

where $\mathbf{E}$ is the vector of electric field and is defined as $\mathbf{E} = E_3 = -\dfrac{v}{t^p}$. Substituting the respective terms from the constitutive relations (9) gives,

$$W_{ie} = \frac{1}{2}\int_{A^p} E_3(\mathbf{e}'^{T}\overline{\boldsymbol{\varepsilon}}^L + \mathbf{e}'^{T}\overline{\boldsymbol{\varepsilon}}^{NL} + \eta_{33}E_3)\,dA^p \tag{24}$$

Variation of the internal electrical energy in Hamilton's principle is derived using,

$$\delta W_{ie} = \frac{\partial W_{ie}}{\partial \mathbf{X}}\delta\mathbf{X} + \frac{\partial W_{ie}}{\partial v}\delta v \tag{25}$$

4.3 Kinetic energy of the system

The total kinetic energy term in (16) can be written as follows,

$$T = \frac{1}{2}\int_{V^s} \rho^s\dot{\mathbf{u}}_a^T\dot{\mathbf{u}}_a\,dV^s + \frac{1}{2}\int_{V^p} \rho^p\dot{\mathbf{u}}_a^T\dot{\mathbf{u}}_a\,dV^p \tag{26}$$

where ρ^s and ρ^p are the densities of the substructure and the piezoelectric layer, respectively and $\mathbf{u}_a$ is the absolute displacement vector including the base excitation and deformations of the laminate, expressed as follows,

$$\mathbf{u}_a = \left[u_x^0 - z\frac{\partial w}{\partial x}, u_y^0 - z\frac{\partial w}{\partial y}, w + w_b \right] \tag{27}$$

where u_x^0, u_y^0 are in-plane displacements and assumed to be zero, w_b is the base excitation function and w is the deflection of the laminate and approximated as

$$w = \frac{1}{2}(ax^2 + by^2 + cxy) = \begin{bmatrix} \frac{x^2}{2} & \frac{y^2}{2} & \frac{xy}{2} \end{bmatrix} \begin{bmatrix} a \\ b \\ c \end{bmatrix} = \mathbf{g}^T\mathbf{a} \tag{28}$$

Substituting (27) and (28) into (26) and taking variation of the kinetic energy gives,

$$\int_{t_1}^{t_2} \delta T\, dt = \int_{t_1}^{t_2} (-\ddot{\mathbf{a}}^T\mathbf{M} - \ddot{w}_b\mathbf{M}_b)\delta\mathbf{a}\, dt \tag{29}$$

where $\mathbf{M}$ and $\mathbf{M}_b$ are the inertial and base excitation mass matrices, respectively, defined as

$$\mathbf{M} = \int_V \rho(z^2(\mathbf{G}_x + \mathbf{G}_y) + \mathbf{G})\, dV \tag{30}$$

$$\mathbf{M}_b = \int_V \rho\mathbf{g}^T\, dV \tag{31}$$

where

$$\mathbf{G}_x = \mathbf{g}_{,x} \otimes \mathbf{g}_{,x}\,;\ \mathbf{G}_y = \mathbf{g}_{,y} \otimes \mathbf{g}_{,y}\,;\ \mathbf{G} = \mathbf{g} \otimes \mathbf{g}$$

and $\mathbf{g}_{,x}$ indicates $\frac{\partial\mathbf{g}}{\partial\mathbf{x}}$. Applying the superposition principle, the total mass matrices including substructure and piezoelectric mass matrices can be derived,

$$\mathbf{M} = \mathbf{M}^s + \mathbf{M}^p = \int_{V^s} \rho^s(z^2(\mathbf{G}_x + \mathbf{G}_y) + \mathbf{G})\, dV^s + \int_{V^p} \rho^p(z^2(\mathbf{G}_x + \mathbf{G}_y) + \mathbf{G})\, dV^p \tag{32}$$

$$\mathbf{M}_b = \mathbf{M}_b^s + \mathbf{M}_b^p = \int_{V^s} \rho^s\mathbf{g}^T\, dV^s + \int_{V^p} \rho^p\mathbf{g}^T\, dV^p \tag{33}$$

4.4 Non-conservative work, W_{nc}

The final term in (16), the non-conservative work due to electrical charge output is defined as follows

$$\delta W_{nc} = \delta W_{nc}^p = Q(t)\,\delta v(t) \tag{34}$$

4.5 Governing equations

By having all terms of Hamilton's principle (16) as multipliers of virtual in-plane deformation and curvature coefficients ($\delta\mathbf{X}$) and virtual voltage (δv) and factorizing $\delta\mathbf{X}$ and δv, their multipliers should be zero in the time interval t_1 to t_2. Consequently, the governing equations of the problem are derived as follows,

$$\begin{bmatrix} \mathbf{0} & \mathbf{0} \\ \mathbf{0} & \mathbf{M} \end{bmatrix}\begin{bmatrix} \ddot{\mathbf{d}} \\ \ddot{\mathbf{a}} \end{bmatrix} + \begin{bmatrix} \mathbf{K}_{11} & \mathbf{K}_{12} \\ \mathbf{K}_{21} & \mathbf{K}_{22} \end{bmatrix}\begin{pmatrix} \mathbf{d} \\ \mathbf{a} \end{pmatrix} + \begin{bmatrix} \boldsymbol{\theta}_d \\ -\boldsymbol{\theta}_a \end{bmatrix}v = \begin{bmatrix} 0 \\ \mathbf{M}_b\ddot{w}_b \end{bmatrix} \tag{35}$$

$$-\boldsymbol{\theta}_d\dot{\mathbf{d}} + \boldsymbol{\theta}_a\dot{\mathbf{a}} + \frac{C_p\dot{v}}{t^p} + \frac{v}{R} = 0 \tag{36}$$

where $\mathbf{d}$ and $\mathbf{a}$ are the in-plane strain coefficients vector and the curvatures, respectively, and,

$$\mathbf{K}_{11} = \int_{A^s} \overline{\boldsymbol{\varphi}}^T \mathbf{A}^s \overline{\boldsymbol{\varphi}} \, dA^s + \int_{A^p} \overline{\boldsymbol{\varphi}}^T \mathbf{A}^p \overline{\boldsymbol{\varphi}} \, dA^p \tag{37}$$

$$\mathbf{K}_{12}^T(\mathbf{a}) = \int_{A^s} -\mathbf{a}^T \mathbf{B}^s \overline{\boldsymbol{\varphi}} + \mathbf{f}^T \mathbf{A}^s \overline{\boldsymbol{\varphi}} - \Delta T \overline{\alpha} (\mathbf{A}^s + \mathbf{B}^s) \overline{\boldsymbol{\varphi}} \, dA^s + \\ \int_{A^p} -\mathbf{a}^T \mathbf{B}^p \overline{\boldsymbol{\varphi}} + \mathbf{f}^T \mathbf{A}^p \overline{\boldsymbol{\varphi}} \, dA^p \tag{38}$$

$$\mathbf{K}_{21}^T(\mathbf{a}) = \int_{A^s} -\overline{\boldsymbol{\varphi}}^T \mathbf{B}^s + \overline{\boldsymbol{\varphi}}^T \mathbf{A}^s \mathbf{f}_{,\mathbf{a}} \, dA^s + \\ \int_{A^p} -\overline{\boldsymbol{\varphi}}^T \mathbf{B}^p + \overline{\boldsymbol{\varphi}}^T \mathbf{A}^p \mathbf{f}_{,\mathbf{a}} \, dA^p \tag{39}$$

$$\mathbf{K}_{22}^T(\mathbf{a}) = \int_{A^s} \mathbf{a}^T \mathbf{D}^s - \mathbf{f}^T \mathbf{B}^s - \mathbf{a}^T \mathbf{B}^s \mathbf{f}_{,\mathbf{a}} + \mathbf{f}^T \mathbf{A}^s \mathbf{f}_{,\mathbf{a}} \, dA^s + \\ \int_{A^p} \mathbf{a}^T \mathbf{D}^p - \mathbf{f}^T \mathbf{B}^p - \mathbf{a}^T \mathbf{B}^p \mathbf{f}_{,\mathbf{a}} + \mathbf{f}^T \mathbf{A}^p \mathbf{f}_{,\mathbf{a}} \, dA^p - \\ \int_{A^s} \Delta T \, \overline{\alpha} ((\mathbf{A}^s + \mathbf{B}^s) \mathbf{f}_{,\mathbf{a}} - (\mathbf{B}^s + \mathbf{D}^s)) \, dA^s \tag{40}$$

$$\boldsymbol{\theta}_d = \frac{t^p + 1}{2t^p} \int_{A^p} \mathbf{e}^T \overline{\boldsymbol{\varphi}} \, dA^p \tag{41}$$

$$\boldsymbol{\theta}_a = \frac{t^p + 1}{2t^p} \int_{A^p} \mathbf{e}^T (\frac{\overline{t}}{2} - \mathbf{f}_{,\mathbf{a}}) \, dA^p \tag{42}$$

where $\mathbf{f}_{,\mathbf{a}}$ denotes $\frac{\partial \mathbf{f}}{\partial \mathbf{a}}$.

The in-plane strain coefficients $\mathbf{d}$ can be obtained from the first equation of (35) in terms of curvatures $\mathbf{a}$. Substituting $\mathbf{d}$ into the second equation of (35) and (36) gives,

$$\begin{cases} \mathbf{M}\ddot{\mathbf{a}} + \mathbf{K}(\mathbf{a}) + (\mathbf{k}_{\theta 1}^T(\mathbf{a})\boldsymbol{\theta}_d - \boldsymbol{\theta}_a)v = \mathbf{M}_b \ddot{w}_b \\ (-\boldsymbol{\theta}_d^T \mathbf{k}_{\theta 2}(\dot{\mathbf{a}}) + \boldsymbol{\theta}_a \dot{\mathbf{a}}) + (\frac{C^p}{t^p} + C_d)\dot{v} + \frac{v}{R} = 0 \end{cases} \tag{43}$$

where,

$$\mathbf{K}(\mathbf{a}) = \mathbf{K}_{22}(\mathbf{a}) - \mathbf{K}_{21}(\mathbf{a}) \mathbf{K}_{11}^{-1} \mathbf{K}_{12}(\mathbf{a})$$
$$\mathbf{k}_{\theta 1}(\mathbf{a}) = -\mathbf{K}_{21}(\mathbf{a}) \mathbf{K}_{11}^{-1}$$
$$\mathbf{k}_{\theta 2}(\dot{\mathbf{a}}) = -\mathbf{K}_{11}^{-1} \mathbf{K}_{12}(\dot{\mathbf{a}})$$
$$C_d = \boldsymbol{\theta}_d \mathbf{K}_{11}^{-1} \boldsymbol{\theta}_d \tag{44}$$

where $\mathbf{K}(\mathbf{a})$ is the mechanical tangential stiffness matrix, $\mathbf{k}_{\theta 1}^T(\mathbf{a})\boldsymbol{\theta}_d$ and $\boldsymbol{\theta}_a$ are the nonlinear electromechanical vectors related to axial deformations coefficients $\mathbf{d}$ and curvatures $\mathbf{a}$, respectively. In addition, the electromechanical nonlinear term $\boldsymbol{\theta}_d^T \mathbf{k}_{\theta 2}(\dot{\mathbf{a}})$ in the sensing equation of (43) can be interpreted as the product of coupling coefficients and acceleration in the linear case. It is noted that in Hyer's model $\mathbf{e}^T \mathbf{f}_{,\mathbf{a}} = \mathbf{0}$, therefore, the nonlinear term in $\boldsymbol{\theta}_a$ vanishes and (41) can be simplified as,

$$\boldsymbol{\theta}_a = \frac{t^p + 1}{2t^p} \int_{A^p} \frac{\overline{t}}{2} \mathbf{e}^T \, dA^p \tag{45}$$

8

5 LAMINATES WITH ARBITRARY SHAPES

In this work we look to generalize the above model to consider arbitrary planforms. To achieve this, a rectangular design domain is considered and discretized to the number of regular elements as shown in Figure 2. A very fine grid therefore provides a close approximation to a shape defined by a smooth boundary. Each element is considered to be represented either by one for solid areas or zero for voids, which becomes the multiplier for each elemental properties. Since every element should satisfy the dynamic equilibrium (16) in order to have equilibrium of the whole structure, the expressions derived in the previous section can be applied for each element. Therefore, the tangential stiffness and mass matrices in (35) may be written in the form of,

$$\mathbf{K} = \sum_{e=1}^{n} \mu_e \mathbf{K}_e \; ; \; \mathbf{M} = \sum_{e=1}^{n} \mu_e \mathbf{M}_e \qquad (46)$$

where μ_e is the elemental multiplier, one for solid elements and zero for voids. It is noted that the density of the grid has no discernable effect on computation time as no solving is performed on an element by element basis. Furthermore a single shape function is used and thus no continuity conditions between elements are required.
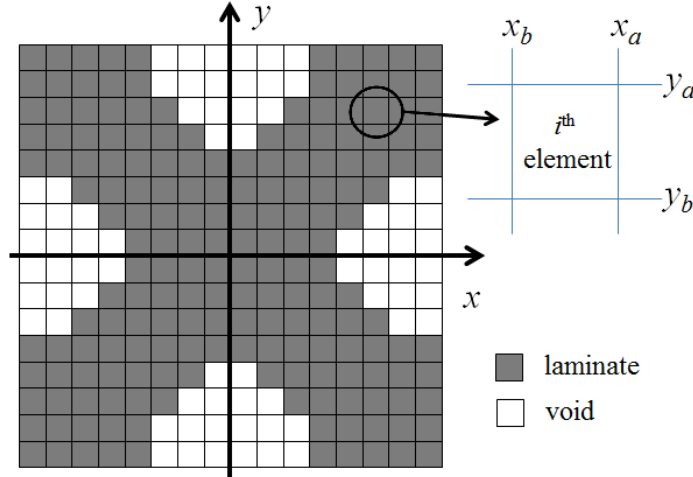

Figure 2. Discretization of an example bistable laminate planform.

6 MODELLING SQUARE AND CRUCIFORM SHAPES

We investigate the dynamic response and electrical output of the a square and a cruciform shapes using the analytical model. The square Carbon Fiber Reinforced Polymer (CFRP) laminate has dimensions 150×150×0.34 mm and a cruciform (+ shape) is cut from the square laminate with 15% of the total area removed, shown in Figure 3. The laminates are of stacking sequence [0/90]$_T$ and material properties are defined in Table 1. Bonded to the top surface of the laminates is a single Macro Fibre Composite (MFC) piezoelectric element (M-2814-P2, [15]) of dimensions 28×14×0.3mm, polarized through its thickness with an experimentally measured capacitance of 33nF and material properties as defined in Table 1.

The dynamic model results for the square and the cruiciform laminates are obtained by starting the dynamic simulation at stable state A of Figure 4. The results for three different levels of excitations are shown in Figures 5 and 6. Figure 5 shows simulations of the corner displacement, velocity and output voltage histories of the square laminate as the vibration frequency is linearly swept between 45Hz to 65Hz at 3g, 6.25g and 9g amplitude. Theses amplitudes are chosen to observe three distinctive dynamic modes, i.e. 3g for single-well

oscillations, 6.25g where the first snap-through is observed and 9g for double-well oscillations. Figure 6 shows simulations of the cruciform laminate responses as vibration frequency is swept within the range of 55Hz to 75Hz.

Property		T800/M21 (laminate)	M2814-P2(piezoelectric)[15]
Longitudinal elastic modulus, E_{11} (GPa)		178	30.3
Transverse elastic modulus, E_{22} (GPa)		8.15	15.9
Shear modulus, G_{12} (GPa)		5.2	5.5
Poisson's ratio, v_{12}		0.35	0.31
Longitudinal thermal expansion coefficient, α_1	(˚C^{-1})	-9×10^{-8}	N/A
Transverse thermal expansion coefficient, α_2	(˚C^{-1})	2.65×10^{-5}	N/A
Dielectric constant d_{31}	(C/N)	N/A	170×10^{-12}

Table 1: Laminate and piezoelectric material properties.

(a)   (b)
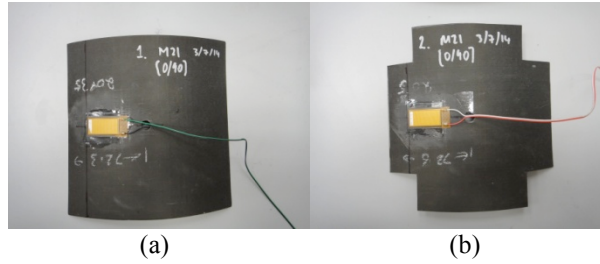
Figure 3. (a) Square and (b) cruciform laminates with bonded piezoelectric elements. Overall laminate dimension is 150×150mm.
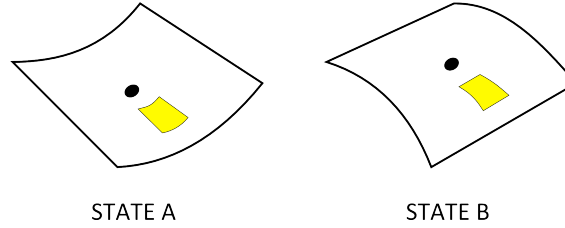

STATE A   STATE B

Figure 4. Stable states A and B defined with reference to the position and orientation of the piezoelectric element.

For the square laminate the initial stable state changed from state A to state B at an acceleration level of 6.25g and a frequency of 55Hz. The cruciform laminate exhibits an initial snap through event at a higher acceleration level, 7g, and higher frequency, 62Hz. Since the resonant frequency of the harvester is proportional to $\sqrt{k/m}$, the higher resonant frequency of the cruciform device indicates that the effects of mass (*m*) reduction on removing material from the corners of the laminate is greater than those of decrease in stiffness (*k*). Figures 5 and 6 (g-h) show that the model is able to recognize double well oscillations in both laminates at 9g level of excitations. Due to differences in the mass distribution of the square and cruciform laminates, the dynamic responses show some differences and offers a route to tailor the harvester response. For example, at a vibration level of 9g the root mean square (rms) voltages are 9.5V (Figure 5c) and 8.5V (Figure 6c) for the square and cruciform laminates respectively. The higher voltage of the square laminate is likely to be due to the increased mass at the laminate corners, thereby leading to a greater effective forcing function during oscillation. Similar maximum output voltages are observed at low levels of excitation, 3g, for both types of laminate.
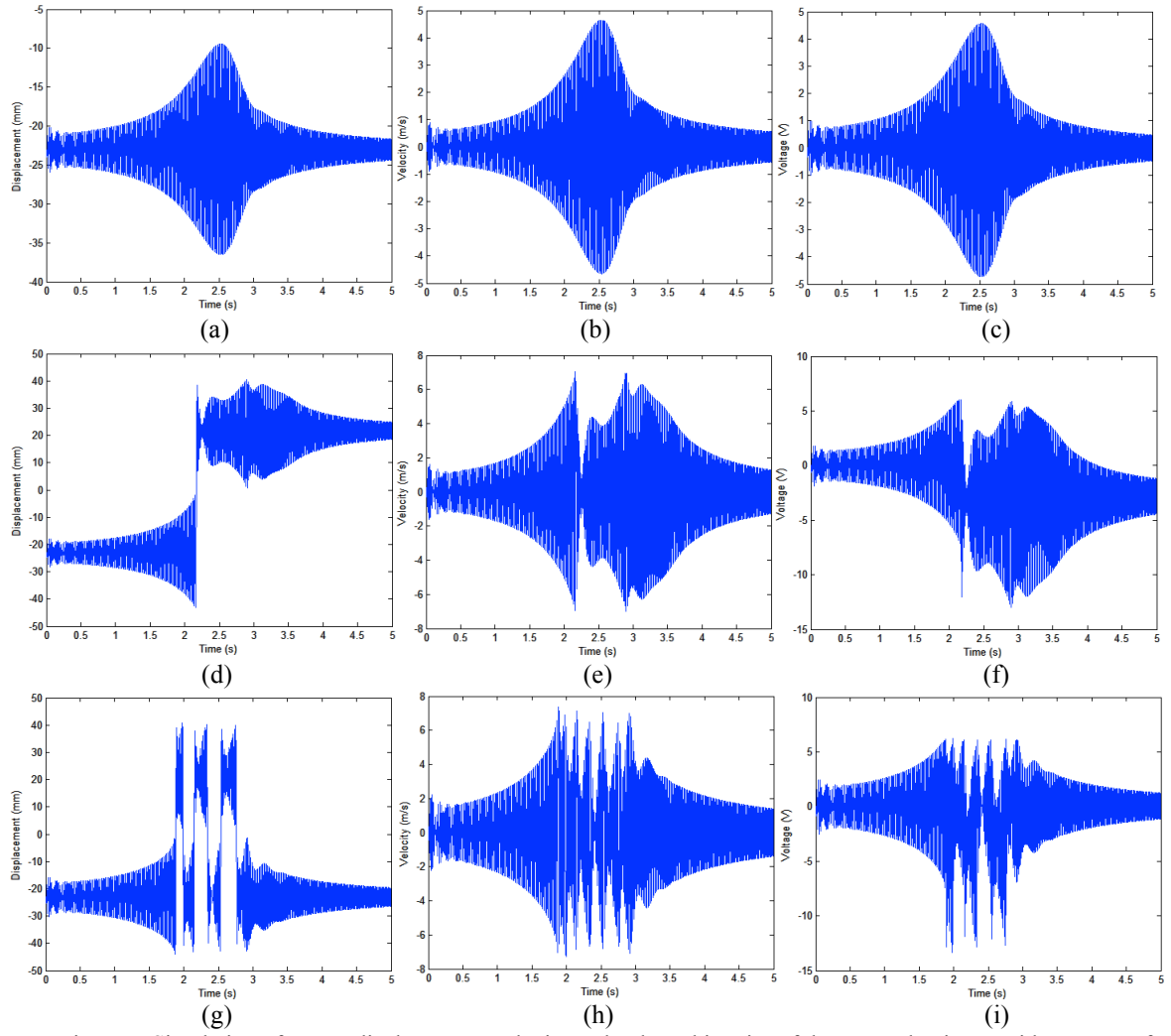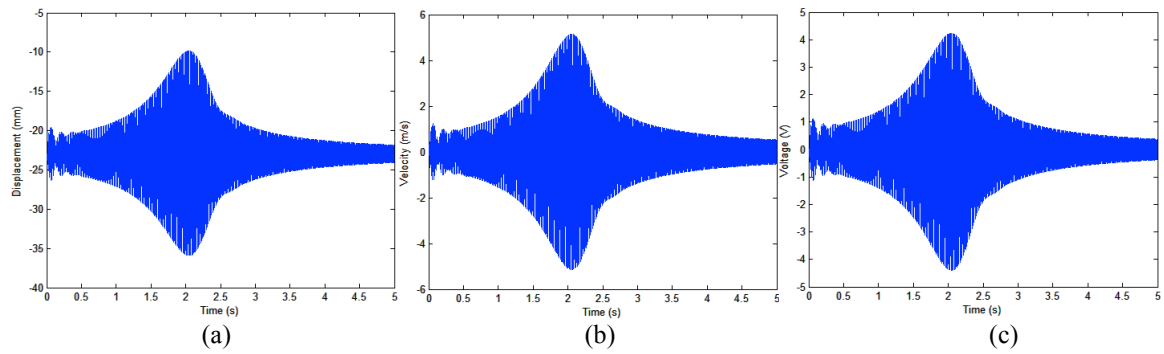
Figure 5. Simulation of corner displacement, velocity and voltage histories of the square laminate, with a sweep of drive frequencies within the range of 45Hz to 65Hz, for the excitation amplitudes of (a-c) 3g (single-well oscillations) (d-e) 6.25g (first snap through event) (g-i) 9g (double-well oscillations).
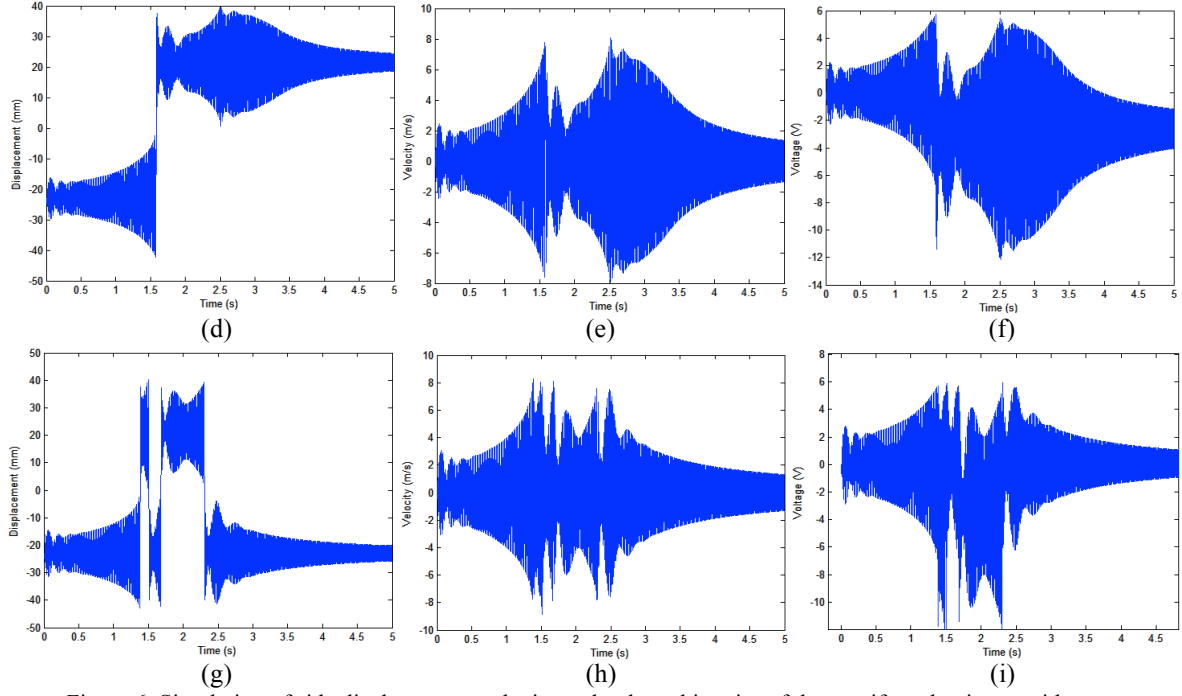
Figure 6. Simulation of side displacement, velocity and voltage histories of the cruciform laminate, with a sweep of drive frequencies within the range of 55Hz to 75Hz, for the excitation amplitudes of (a-c) 3g (single-well oscillations) (d-e) 7g (first snap-through event) (g-i) 9g (double-well oscillations).

7. EXPERIMENTAL AND MODELING COMPARISONS

In this section, the analytical model presented in this paper is compared against experimental tests. The energy harvester is mounted at its center on an electrodynamic shaker. The shaker input is a sine wave from a signal generator and power amplifier. A laser displacement sensor is used to measure the vibration amplitude. This measurement forms part of a computer-controlled feedback loop to maintain constant acceleration during frequency sweeps.

We first measure the maximum deflection of the static cured shapes of the laminates, labeled A and B (see figure 4), and compare with the proposed model. The experimental and modeling results are compared in Table 2 in two stable states. The results show up to 4% in stable shape A and up to 10% discrepancies in stable shape B in both square and cruciform laminates. In fact, around 10% or less discrepancies between experimental and analytical models are consistent with the previous literature on square or rectangular laminates. Therefore, the analytical model developed in this paper offers a good approximation for an arbitrary shape laminates.

Shape		Square		Cruciform	
Stable state		A	B	A	B
Experiment	(mm)	21	19	22	19
Model	(mm)	21.2	21	21.2	20.9
Discrepancies	%	1	10	4	9

Table 2: Maximum deflections of the laminates.

Figure 7 shows the experimental and model maximum power results, recorded for different peak accelerations 2g to 10g for the cruciform shaped laminate. The load resistance R_l is measured experimentally as 87 kΩ, corresponding to an optimal impedance for a

piezoelectric's capacitance, C_p ($2\pi f C_p R_l = 1$) at a frequency, f of 52Hz. The power output from the single MFC is determined by V_{rms}^2/R_l. The results show broad agreement between the model and experiment in both magnitude and trend, although discrepancies up to 30 percent between the model and experimental measurements are observed. Possible reasons for these discrepancies include natural deviation in mechanical, electrical and piezoelectric properties from datasheet values, local stiffening in the region of the piezoelectric element, incomplete strain transfer between the laminate and the piezoelectric patch, or unaccounted losses.
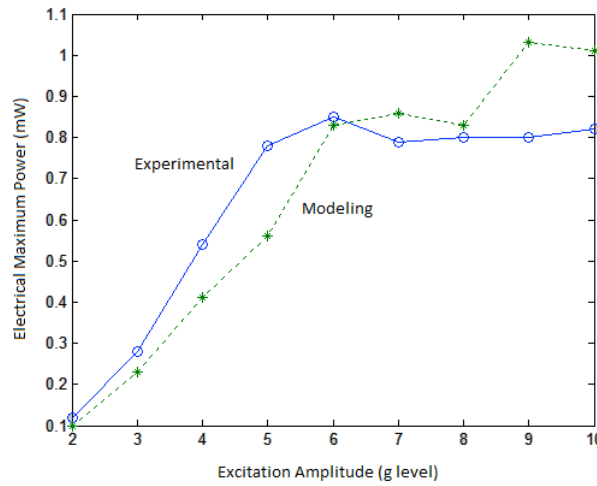

Figure 7. Comparison of maximum experimental and modeling power outputs for different excitation amplitudes

7   CONCLUSION

This paper presents an analytical model for dynamics of piezoelectric bistable laminates with arbitrary shapes. The governing equations of the nonlinear dynamic system are derived based on Hamilton's principle and the Hyer's model is used to approximate the strain field of laminates. The model is then extended to consider arbitrary shapes by discretizing an overall square domain and considering zero properties for void elements. Predictions of the cured shapes of two square and cruciform laminates have been experimentally compared and 1-10% discrepancies are observed between modelling and experiments. Transient analysis is performed using the Runge-Kutta method and the dynamic response and output voltage of the model are demonstrated for both composite laminates. The maximum power outputs are experimentally compared for the cruciform laminate and the results show broad agreement between the model and experiment in both magnitude and trend although discrepancies as much as 30% was observed. Uncertainties in material properties from datasheet values, local stiffening in the region of the piezoelectric element and incomplete strain transfer between the laminate and the piezoelectric patch might be some reasons of these discrepancies. Further investigations are underway to gain a better understanding of these discrepancies.

REFERENCES

[1] S.H. Ju, H.T. Lin, J.Y.Huang, Dominant frequencies of train-induced vibrations, *Journal of Sound and Vibration*, **319**(1-2), 247-259, 2009.

[2] Q. Zhu, M. Guan, Y.He, Vibration energy harvesting in automobiles to power wireless sensors, *International Conference on Information and Automation Conference Proceedings*, Shenyang China, 349-354, 2012.

[3] O. J. Wood, C. A. Featherston, D. Kennedy, M. Eaton, R. Pullin, Optimised vibration energy harvesting for aerospace applications, *Key Engineering Materials – Structural Health Monitoring II*, **518**, 246-260, 2012.

[4] S. Zhou, J. Cao, A. Erturk, J. Lin, Enhanced broadband piezoelectric energy harvesting using rotatable magnets, *Applied Physics Letters*, **102**(173901), 1-4, 2013.

[5] M. W. Hyer, Calculations of the room-temperature shapes of unsymmetric laminates, *Journal of Composite Materials*, 15(July), 296-310, 1981.

[6] A. F. Arrieta, P. Hagedorn, A. Erturk, D.J. Inman, A piezoelectric bistable plate for nonlinear broadband energy harvesting, *Applied Physics Letters*, **97**(10), 1-3, 2010.

[7] D.N. Betts, H.A. Kim, C.R. Bowen, D.J. Inman, The optimal configuration for broadband energy harvesting using bistable phenomenon, *Applied Physics Letters*, **100**(114104), 1-4, 2012.

[8] D.N. Betts, H.A. Kim, C.R. Bowen, Preliminary study of optimum piezoelectric cross-ply composites for energy harvesting, *Smart Materials Research*, 1-8, 2012.

[9] M.L. Dano, M.W. Hyer, Thermally induced deformation behavior of unsymmetric laminates, *International Journal of Solids and Structures*, **35**(17), 2101-2120, 1998.

[10] M.L. Dano, M.W. Hyer, SMA-induced snap-through of unsymmetric fiber-reinforced composite laminates, *International Journal of Solids and Structures*, **40**(22), 5949-5972, 2003.

[11] L. Ren, A. Parvizi, A model for shape control of cross-ply laminated shells using a piezoelectric actuator, *Journal of Composite Materials*, **40**(14), 1271-1285, 2006.

[12] D.N. Betts, C.R. Bowen, H.A. Kim, R. Guyer, P. Le Bas, D. Inman, Modeling the dynamic response of bistable composite plates for energy harvesting, *55th AIAA Structures, Strucutral Dynamics, and Material Conference,* Jan 2014.

[13] S. Tawfik, D.S. Dancila, E. Armanios, Planform effects upon the bistable response of cross-ply composite shells, *Composites Part A: Applied Science and Manufacturing*, **42**(7), 825-833, 2011.

[14] A.F. Arrieta, O. Bilgen, M.I. Friswell, P. Ermanni, Modelling and configuration control of wing-shaped bi-stable piezoelectric composites under aerodynamic loads, *Aerospace Science and Technology*, **29**(1), 453-461, 2013.

[15] Smart Material Corp., www.smart-material.com/MFC-product-main.html, Jan 2014.